

Photoinduced electron transfer and geminate recombination in the group head region of micelles

Ksenija Glusac, Alexei Goun, and M. D. Fayer^{a)}

Department of Chemistry, Stanford University, Stanford, California 94305

(Received 27 February 2006; accepted 21 June 2006; published online 3 August 2006)

A pump-probe spectroscopic study of photoinduced forward electron transfer and geminate recombination between donors and acceptors located in the head group regions of micelles is presented. The hole donor is octadecyl-rhodamine B (ODRB) and the hole acceptor is *N,N*-dimethyl-aniline (DMA). The experiments are conducted as a function of the DMA concentration in the dodecyltrimethylammonium bromide and tetradecyltrimethylammonium bromide micelles. In spite of the fact that the absorptions of both the ODRB radical and ground state bleach spectrally overlap with the ODRB excited state absorption, a procedure that makes it possible to determine the geminate recombination dynamics is presented. These experiments are the first to measure the dynamics of geminate recombination in micelles, and the experiments have two orders of magnitude better time resolution than previous studies of forward transfer. The experimental data are compared to statistical mechanics theoretical calculations of both the forward transfer and the geminate recombination. The theory includes important aspects of the topology of the micelle and the diffusion of the donor-acceptors in the micelle head group region. A semiquantitative but nonquantitative agreement between theory and experiments is achieved. © 2006 American Institute of Physics. [DOI: 10.1063/1.2227392]

I. INTRODUCTION

Although the main solvent in biological systems is water, most biochemical reactions occur at interfaces or in confined protein hydrophobic pockets. These pockets increase reactivity by bringing the reactants in close proximity and by tuning the solvent properties, such as viscosity, polarity, and pH.¹⁻³ To mimic biological systems, a large number of self-organized molecular assemblies, such as micelles,⁴ reverse micelles,⁵ microemulsions,⁶ and gels,^{7,8} have been designed and studied. In a manner akin to biological systems, the artificial molecular assemblies influence the reactivity of the molecules imbedded within by changing the solvent properties and confining the reactants near each other.⁹ These artificial systems can be viewed as simplified models for the study of factors influencing biochemical reactions. Furthermore, the control of chemical reactions by means of molecular assemblies may find utility in devices, such as solar cells, where the molecular assemblies can be used to inhibit the recombination of radicals produced upon photoexcitation.^{10,11}

A wide variety of experimental techniques are being used to study molecular assemblies. Structural elucidation, such as determination of the sizes of assemblies or the location of probes within molecular assemblies can be determined by x-ray and neutron scattering¹² and NMR spectroscopy.¹³ Other studies are focused on the properties of the solvent within the molecular assembly.^{14,15} In most of the molecular assemblies, the aggregate is hydrophobic and submerged in water. The interface between the molecular assem-

bly and bulk water produces a “hybrid” solvent with properties substantially different from those of bulk water.

The dynamics of a specific reaction in a molecular assembly will be influenced by the properties of the assembly. The properties of the “local” solvent, the local concentration of reactants, and their diffusion coefficients will play important roles in modifying the reaction dynamics from the dynamics that would occur in a bulk solvent. Previous studies on reaction dynamics in molecular assemblies have compared the reaction rates in liquid with the rates in molecular assemblies.¹⁶⁻¹⁸ Frequently, this approach gives an excellent qualitative description of the influence of the molecular assembly on the reaction kinetics, but it may not yield information on specific parameters that influence the rate of reaction.

Electron transfer is a fundamental process that takes place in chemical and biological systems.¹⁹ In biological systems and in many chemical systems, electron transfer occurs between organic and organometallic molecules. Photoinduced electron transfer involving organic molecules is being widely studied for applications in solar energy conversion.²⁰ A detailed statistical mechanics theoretical model for photoinduced forward electron transfer^{21,22} and the combined problem of forward transfer and geminate recombination in liquids has been tested and applied to the analysis of experiments.²³⁻³³ The forward transfer/geminate recombination theory calculates the decay curves for the excited states and the radical species in a system of diffusing donors and acceptors. The theory accounts for the effect of solvent molecules on the distribution of acceptors around the donor (radial distribution function), as well as the effect of solvent molecules on the donor/acceptor diffusion coefficients at

^{a)}Electronic mail: fayer@stanford.edu

close approach (hydrodynamic effect^{34,35}).^{30,31} The theory for photoinduced forward electron transfer and geminate recombination in liquids was extended to the donors and acceptors in the head group regions of micellar systems.³⁶⁻⁴¹ Here, the donor/acceptor distribution and diffusive motion reflect the restricted geometry of a micelle, while the dielectric properties of the solvent were modeled as a three region system, consisting of core, head group, and bulk water, each with distinct dielectric properties.^{36,37} This is in contrast to liquids in which the dielectric properties are treated as a single continuum.

In this paper, we present a study of photoinduced electron transfer and the first measurements of geminate recombination in micelles. The systems studied are the hole donor octadecyl-rhodamine B (ODRB) and the hole acceptor *N,N*-dimethyl-aniline (DMA) in micelles made of dodecyltrimethylammonium bromide (DTAB) and tetradecyltrimethylammonium bromide (TTAB). Photoexcitation of the low concentration ODRB causes an electron to transfer from the high concentration DMA to ODRB. Because ODRB is in low concentration and is photoexcited, we consider it to be the donor, in this case, a hole donor, and DMA, which is in high concentration, to be a hole acceptor. In previous studies of this system^{36,37} forward electron transfer was studied with ~ 100 ps time resolution. Here both forward electron transfer and geminate recombination are measured with subpicosecond time resolution.

The dynamics of the forward electron transfer and geminate recombination are studied using spectrally resolved pump-probe spectroscopy. Forward electron transfer is monitored by observing the decay of the initially prepared excited state population by measuring the time dependence of the stimulated emission in the fluorescence region of the donor. To measure the geminate recombination, it is necessary to observe either the decay of the radicals that are generated by forward electron transfer or the decay of the ground state bleach that is created upon electron transfer. The absorptions of both the ODRB radical species and the ground state bleach spectrally overlap with ODRB excited state excited state absorptions. This creates a problem because the excited state absorption and the portion of the ground state bleach that arises from the generation of excited states decay with dynamics that are related to the forward transfer, but the radicals and the portion of the ground state bleach that is produced by the existence of radicals decay with dynamics related to the geminate recombination. We have developed and presented an experimental method that allows us to determine the dynamics of the geminate recombination in spite of the spectral overlaps.

A statistical mechanical model is used to calculate the time dependent survival probabilities for the donor in its excited state and for radicals produced following electron transfer. The experimental data for the forward transfer and geminate recombination are fitted to the model. Some of the parameters needed for the calculation are known at least approximately. It is found that the previous parameters obtained from fits to the forward transfer data for $t > 50$ ps do not reproduce the short time data. New fits give reasonable agreement between the model calculations and the data for

both forward and backward transfer, but there are inconsistencies in the fits that may arise from aspects of the micelle structure and dynamics in micelles that are not accounted for by the theoretical model.

II. EXPERIMENT PROCEDURES

A. Sample preparation

The details of the sample preparation were reported previously.^{36,38} DTAB and TTAB were obtained from Aldrich. To assure that the micelles are spherical and monodispersed, DTAB/TTAB concentrations were kept just above the critical micelle concentration.^{38,42} The micelle concentration was $206 \mu\text{M}$ for all micelle systems. ODRB was obtained from Molecular Probes. The ODRB concentration was $20 \mu\text{M}$, which ensured that there is at most one ODRB per micelle, which eliminates the possibility of electronic excitation transfer between ODRBs. DMA was obtained sealed under nitrogen from Aldrich and used without further purification. For each of the micelle systems, four samples were prepared: one that contained only ODRB and three that also had DMA of varying concentrations (3, 6, and 12 mM DMA). Since DMA is somewhat soluble in water, only a fraction of DMA molecules binds to the micelle surface. A value of 57% bound DMA was obtained for CTAB (hexadecyltrimethylammonium bromide) micelles.³⁶ We assume that the same fraction of DMA molecules binds to DTAB and TTAB micelles although this number is allowed to vary somewhat when fits to the data are performed to test the sensitivity of the results.

B. Pump-probe experiment

Pump-probe experiments were performed using a 1 kHz Ti:sapphire regenerative amplifier (800 nm) to pump a beta-barium borate (BBO) optical parametric amplifier to produce ~ 1.9 and $\sim 1.3 \mu\text{m}$ light. The leftover 800 nm pulses were summed with the $\sim 1.9 \mu\text{m}$ pulses in another BBO crystal to produce 565 nm pump pulses. A small part of the pump pulse was beam split to use as one of the probe pulse colors. A second probe pulse was produced by doubling the $\sim 1.3 \mu\text{m}$ in another BBO crystal to produce 630 nm light. The 565 and 630 nm probes were coaligned prior to the sample. Therefore, the two probe pulses interrogated the same spot in the sample. The pump light was chopped at 500 Hz frequency. The energy of pump pulses was $5 \mu\text{J/pulse}$. The pump and probe beams were overlapped in the sample. All of the measurements were conducted at the magic angle geometry. The probe beams were diffracted from a grating after the sample to separate the two colors, and the individual colors were detected by two photodiodes. The signals from the photodiodes were collected using gated integrators, fed to a computer for processing.

In addition, a charge-coupled device (CCD) mounted on a 0.3 m spectrograph was used to take full transient absorption spectra. The transient absorption spectrum is the difference spectrum between the spectrum with the pump pulse and without the pump pulse. These spectra are taken using a "white light" continuum generated in CaF_2 . Two white light probes were used, one that overlapped the pump pulse and

one that did not. These were recorded as two “stripes” on the 100×1360 pixel CCD. The stripe that came from the probe that did not overlap with the pump pulse was used to normalize the white light spectrum. The transient absorption spectra were used to determine the best wavelengths for measuring the dynamics. Only two wavelengths are necessary to determine the forward transfer and geminate recombination dynamics. The wavelengths 565 and 630 nm were determined from the CCD measurements (see below).

The absorption spectrum of the ODRB excited state and its associated ground state bleach overlap with the absorption spectra of radicals and the ground state bleach of the ODRB caused by the generation of the ODRB neutral radical. The analysis of the data to extract the dynamics of the population of radicals that are formed by charge transfer and decay by geminate recombination is complicated by the overlapping spectra. The forward electron transfer is obtained by monitoring the decay of the excited state population, $P_{\text{ex}}(t)$. The excited state population decay is measured using the probe wavelength in the region of stimulated emission, 630 nm, at which there is negligible contribution from radical absorptions. However, the relative time dependent population of the radicals produced by charge transfer, $P_{\text{ct}}(t)$, needs to be extracted from the overlapping spectral contribution of the ODRB excited state absorption and the ODRB ground state bleach, both of which decay as $P_{\text{ex}}(t)$. Because the overlap occurs, we needed to eliminate the contributions to the transient spectrum that decay with $P_{\text{ex}}(t)$.

The excited state absorption and the ground state bleach caused by ODRBs in the excited state are both proportional to the excited state concentration. The proportionality constant for each is the extinction coefficient at a particular wavelength. The spectra of the excited state absorption and the ODRB ground state bleach produced by excited state population and their respective extinction coefficients are the same whether there is electron transfer or not. Therefore, these contributions to the pump-probe signal can be removed by using the transient absorption spectrum of ODRB without DMA acceptors. The ODRB transient absorption spectrum without acceptors is scaled to the excited state population of the sample with acceptors at a given time t and is subtracted. The result is that the contributions of ODRB excited state absorption and the ODRB bleach caused by excited states are removed. The remaining transient absorption spectrum is composed of the ODRB neutral radical absorption and the ODRB ground state bleach caused by population existing as ODRB neutral radicals. (Both the DMA and the DMA radical cation have weak absorptions and do not contribute to the signal. In any case, the DMA radical cation decays through geminate recombination in the identical manner as the ODRB neutral radical. Therefore, neither of these species needs to be considered explicitly.) All of these contributions have the same time dependence, $P_{\text{ct}}(t)$. As charge transfer occurs, the signal from these contributions increases and then decays as geminate recombination occurs.

To obtain the time dependent population of the ODRB neutral radical, we make measurements on two samples at each time point: a sample that contains a given concentration of DMA and a sample without DMA. Each of the samples is

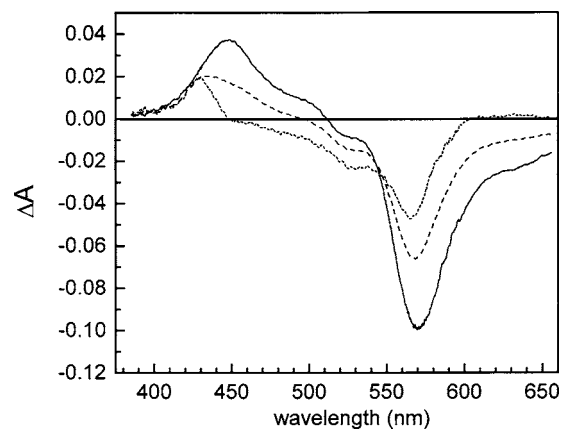


FIG. 1. Transient absorption spectra at 5 ps delay following the pump pulse in DTAB micelles. The solid curve is the transient absorption spectrum ΔA for ODRB with no DMA acceptors. The curve composed of long dashes is the transient absorption spectrum with 12 mM DMA present. The curve composed of the short dashes is the difference of the spectra taken with and without acceptors.

simultaneously probed at two wavelengths: 565 nm, where the maximum radical signal occurs (see below), and 630 nm, where the stimulated emission occurs. We obtained four decays: $S_{565}^W(t)$ (sample with DMA at 565 nm), $S_{630}^W(t)$ (sample with DMA at 630 nm), $S_{565}^N(t)$ (sample with no DMA at 565 nm), and $S_{630}^N(t)$ (sample with no DMA at 630 nm). The experimental excited state probability $P_{\text{ex}}(t)$ and the relative experimental charge transfer (radical) population $P_{\text{ct}}(t)$ were obtained as

$$P_{\text{ex}}(t) = S_{630}^W(t), \quad (1)$$

$$P_{\text{ct}}(t) = S_{565}^W(t) - \frac{S_{565}^N(t)}{S_{630}^N(t)} S_{630}^W(t). \quad (2)$$

To minimize the effects of laser drift in the measurement of the two samples, a sample holder that held both samples was used, and its position was changed by a computer-controlled solenoid. At a given delay line position, corresponding to time t , measurements were first made on one sample, and then the other sample was moved into the pump and probe beams, and measurements were made on it.

III. RESULTS

Figure 1 displays transient absorption spectra taken with the CCD/spectrograph at 5 ps delay following the pump pulse in DTAB micelles. The solid curve is the transient absorption spectrum ΔA for ODRB with no DMA acceptors. The spectrum consists of three distinct features: (i) the positive going ODRB excited state absorption centered at ~ 450 nm, (ii) the negative going ground state bleach centered at ~ 570 nm, and (iii) the negative going ODRB stimulated emission at wavelengths longer than ~ 610 nm (as identified by comparison to the ODRB fluorescence spectrum). The negative going features arise because more light is transmitted through the sample when the pump is on than when the pump is off. In the region of the bleach, more light is transmitted because of ground state depletion. In the region of stimulated emission, the probe pulse emerges with

increased intensity because of gain. The region centered at ~ 450 nm shows an excited state absorption. The region of excited state absorption extends through much of the bleach although it is not apparent because of the very large extinction coefficient associated with the ground state absorption, which gives rise to the bleach. All three transient absorption features are proportional to the number of excited states. The curve composed of long dashes is the transient absorption spectrum at 5 ps with 12 mM DMA present. It displays similar but not identical features to the spectrum in the absence of acceptors. The curve composed of the short dashes is the difference of the spectra taken with and without acceptors at 5 ps. The difference spectrum was obtained after the ODRB only spectrum, and the ODRB/DMA spectrum were normalized to eliminate excited state absorption, stimulated emission, and the ground state bleach produced by the presence of excited states. The resulting spectrum is due only to the presence of radicals and the ground state bleach produced by the population of ODRB neutral radicals. The peak at ~ 430 nm is from the ODRB neutral radical spectrum. The ODRB neutral radicals exhibit an absorption which is in accord with previous pulsed radiolysis studies.⁴³ The bleach arising from the production of radicals is centered at 565 nm. This radical bleach spectrum (short dashes) has no contributions from the excited state absorption, excited state bleach, and stimulated emission. It may have overlapped with radical absorptions, but the radical bleach and the radical absorption both have the same dynamics, $P_{ct}(t)$. Because the radical bleach is approximately a factor of 2 larger than the ODRB radical peak, the radical bleach was used to determine $P_{ct}(t)$.

Figure 2(a) displays data taken in DTAB reverse micelles to 20 ps, a relatively short time period. The Gaussian curve centered at $t=0$ is the instrument response with a full width at half maximum of 320 fs. This is the cross correlation between the 565 nm pump pulse and the 630 nm probe pulse. The short-dashed curve is the data for ODRB with no DMA acceptors. Following the instrument response, the data exhibit no observable decay on this time scale because the only decay mechanism is the excited state lifetime, which is 1.6 ns. The solid curve is the excited state decay $P_{ex}(t)$ with 6 mM DMA taken by probing at 630 nm (stimulated emission) following the 565 nm pump pulse. The decay is substantially faster than the no DMA curve because of forward electron transfer. The long-dashed curve is $P_{ct}(t)$, the normalized charge transfer species concentration. This is obtained in the manner described in Sec. II B. Following the instrument response, $P_{ct}(t)$ continues to grow, reaching a maximum value at ~ 2 ps. At $t=0$, there are excited states but no radicals. As forward transfer occurs, radicals are produced and $P_{ct}(t)$ grows. However, once the radicals are formed, geminate recombination begins to deplete their population. The dynamics are complex. Excited donors that happen to have acceptors close by at $t=0$ will have rapid forward transfer but also rapid geminate recombination. At longer times, forward transfer will occur from excited donors that have acceptors that are further away. Both forward and backward transfers will be slower. At sufficiently long time, only excited donors that have distant acceptors will have survived. If the donor-acceptor separation is sufficiently large, forward

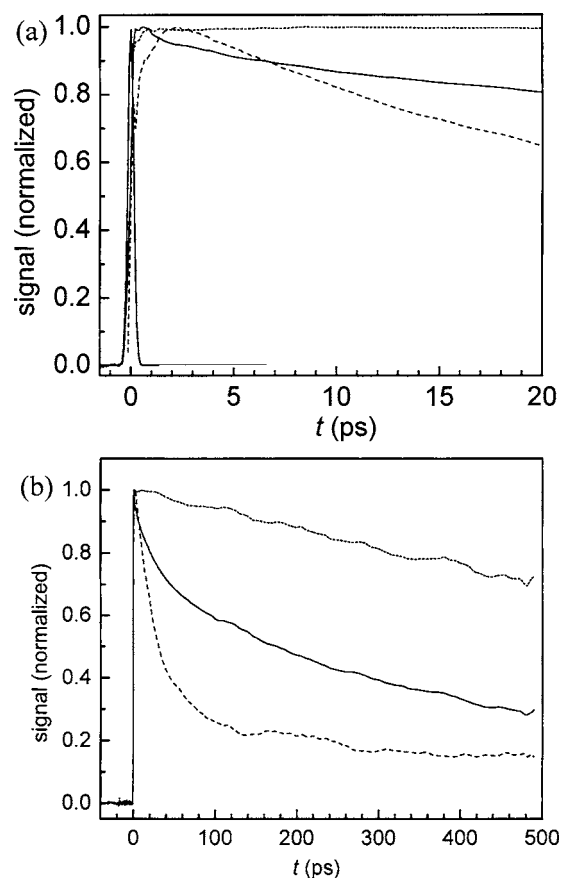


FIG. 2. (a) Data taken in DTAB reverse micelles to 20 ps, a relatively short time period. The Gaussian curve centered at $t=0$ is the instrument response with a full width at half maximum of 320 fs. The short-dashed curve is the data for ODRB with no DMA acceptors. The solid curve is the excited state decay $P_{ex}(t)$ with 6 mM DMA. The long-dashed curve is $P_{ct}(t)$, the normalized charge transfer species concentration. $P_{ct}(t)$ grows in at short time and then decays. (b) The data on a longer time scale. Again, the short-dashed curve is the no acceptor ODRB decay; the solid curve is $P_{ex}(t)$, and the long-dashed curve is $P_{ct}(t)$. By 100 ps there has been substantial geminate recombination, and the remaining geminate recombination slows substantially.

transfer can be much slower than the excited state lifetime, and the decay of $P_{ex}(t)$ will be dominated by the excited state lifetime. However, geminate recombination can still cause $P_{ct}(t)$ to decay. The configuration of donors and acceptors is not static. Their relative positions are constantly changing because of diffusion. Figure 2(b) displays the data on a longer time scale. Again, the short-dashed curve is the no acceptor ODRB decay; the solid curve is $P_{ex}(t)$, and the long-dashed curve is $P_{ct}(t)$. By 100 ps there has been substantial geminate recombination, and the remaining geminate recombination slows substantially.

Figure 3(a) displays the forward electron transfer data, $P_{ex}(t)$, as a function of the DMA acceptor concentration in DTAB micelles. The 0 mM curve is ODRB with no acceptors. At 450 ps shown in the plot, the lifetime decay is $\sim 27\%$. As the concentration increases, forward electron transfer becomes faster, and by 12 mM, $\sim 85\%$ of the excited states have decayed by the combination of the excited state lifetime and electron transfer. At 450 ps, 79% of the initially excited states have undergone forward electron transfer. Figure 3(b) shows the same data as Fig. 3(a), but on a semilog

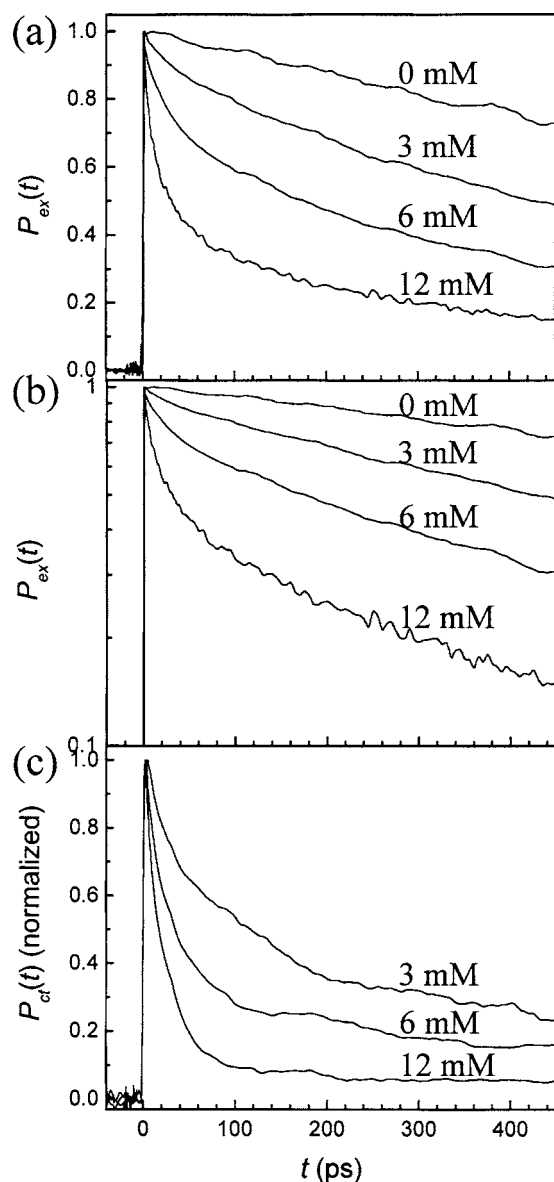


FIG. 3. (a) Forward electron transfer data, $P_{ex}(t)$, as a function of the DMA acceptor concentration in DTAB micelles. (b) The same data as (a) but on a semilog plot. At short times the decays are nonexponential, but at longer times the decays become approximately exponential. Comparing the 0 mM decay curve (no acceptors) to the other curves, it is clear that the decays for the samples with acceptors are not the excited state lifetime at long times. (c) The normalized charge transfer state population $P_{ct}(t)$ for the three DTAB micelle samples with acceptors corresponding to the $P_{ex}(t)$ data shown in (a) and (b). The rate and extent of geminate recombination increase as the concentration of acceptors increases.

plot. At short times the decays are clearly nonexponential, but at longer times the decays become approximately exponential. However, comparing the 0 mM decay curve (no acceptors) to the other curves, it is clear that the decays for the samples with acceptors are not simply the excited state lifetime. All of the decays for the samples with acceptors are significantly faster than the no acceptor decay.

Figure 3(c) displays the normalized charge transfer state population $P_{ct}(t)$ for the three DTAB micelle samples with acceptor concentrations corresponding to the $P_{ex}(t)$ data shown in Figs. 3(a) and 3(b). Figure 3(c) shows that the rate of geminate recombination increases as the concentration of

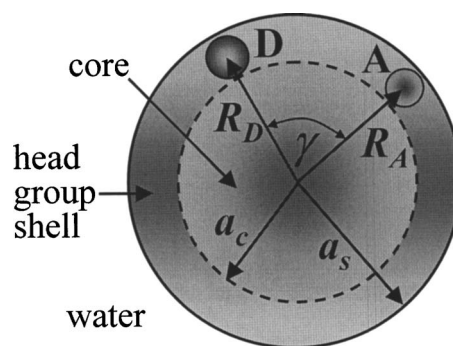


FIG. 4. Schematic showing the physical model of the micelle with donor (D) and acceptor (A) in the head group region of the micelle. γ is the angle between the vectors to the centers of the donor and acceptor. See text.

acceptors increases. Lower concentration produces slower forward transfer that, in general, has the radicals formed further apart. The larger separation results in slower backward transfer and a longer-lived charge transfer population. In the 12 mM sample, the data are nonzero and time independent on the time scale longer than 100 ps. Approximately 5% of the radicals have escaped rapid geminate recombination. The time independence is in spite of the fact that some forward transfer is still occurring. The amount of forward transfer at long times does not result in the production of a sufficient number of radicals to contribute significantly to the long time radical population, within experimental error. The time independent radical population reflects radical pairs that have escaped initial geminate recombination. The species produced by charge transfer, the neutral ODRB radical, and the DMA cation do not have a Coulombic attraction. Therefore, they can more readily diffuse apart than radicals formed by electron transfer between a donor and an acceptor that are initially neutral, which produce oppositely charged radicals with a Coulomb attraction. However, barring other radical quenching mechanisms, on some time scale, radical recombination must occur. The radicals are diffusing in a spherical shell (the head group region, see Fig. 4). Therefore, the radical pair cannot escape to infinity. Eventually, the pair will come in close enough proximity for backward electron transfer to occur. Because there is at most one ODRB per micelle, the recombination will be geminate. The time scale for the recombination following the initial separation is long, on the order of 100 ns, given the mutual diffusion constant of $15 \text{ \AA}^2/\text{ns}$.³⁶

IV. THEORETICAL MODEL AND INPUT PARAMETERS

A. Theoretical model

The details of the theory for electron transfer for a donor and one or more acceptors located in the head group region of micelles has been described previously.³⁶⁻⁴¹ Here the theory will be recounted briefly to provide the equations necessary for the data analysis. The micelle is represented as a sphere of radius R that consists of three regions: the core that contains the nonpolar hydrocarbon chains, the head group region in which donor/acceptor molecules are located, and the surrounding water (see Fig. 4). Experiments have confirmed that the donor and acceptor are in fact located in the

micelle head group region. Fluorescence anisotropy studies of electronic excitation transfer among ODRB molecules in micelles have shown that the chromophore head groups of ODRB are located at the micelle surface in the micelle head group region.⁴⁴ DMA has been shown to reside at the surface of the micelle by means of NMR spectroscopy⁴⁵ and fluorescence spectroscopy.³⁸

Since the acceptor (DMA) is neutral, Coulombic interactions do not exist between donor and acceptors, and their distribution is assumed to be determined by a radial distribution function (see below) in the spherical shell that comprises the head group region. The diffusion of ODRB is negligible compared to the diffusion of the acceptors (DMA) because of its size and the hydrocarbon tail, which is embedded in the micelle core. Diffusion of the acceptors is taken into account. The donor-acceptor separation distance is given by

$$r = 2R \sin(\gamma/2), \quad (3)$$

where R is a “radius of the micelle” taken to be the distance from the center of the micelle to the midpoint of the head group region, and $R=R_D=R_A$ (see Fig. 4).

The diffusion of micelles in the bulk solution is too slow to influence the results, and the concentration of micelles is low enough so that each micelle can be considered a static isolated system. To eliminate the possibility of energy transfer between donor molecules, the concentration of ODRB is such that at most one donor is present in a micelle. The photoexcited ODRB either relaxes back to the ground state or receives an electron from DMA. The radicals generated by forward transfer can backtransfer. We assume that only the geminate recombination is possible. Nongeminate recombination requires an acceptor-acceptor electron hopping mechanism. Acceptor-acceptor hopping is improbable because there is no driving force and there is a significant barrier.

The theory calculates the experimental observables $P_{\text{ex}}(t)$ and $P_{\text{ct}}(t)$ discussed above. $P_{\text{ex}}(t)$ represents the probability that the donor is still in the excited state at time t after the photoexcitation at $t=0$. $P_{\text{ct}}(t)$ is the probability that the radicals produced by forward electron transfer still exist at time t . $P_{\text{ex}}(t)$ has its maximum value of 1 at time $t=0$, and it decreases at a later time due to the radiative or nonradiative relaxation to the ground state and the forward electron transfer. The value of $P_{\text{ct}}(t)$ is zero at time $t=0$. It increases as the forward electron transfer occurs, and it decreases through geminate recombination.

The survival probabilities $S_{\text{ex}}(t|\gamma_0)$ and $S_{\text{ct}}(t|\gamma_0)$ are used as intermediate steps in the calculation. They are quantities describing the dynamics for exactly one donor and one acceptor. $S_{\text{ex}}(t|\gamma_0)$ is the probability that the donor is still excited at time t , given that it is photoexcited at $t=0$ and that the donor and acceptor are separated by a distance corresponding to an angle γ_0 at that time. $S_{\text{ex}}(t|\gamma_0)$ is the solution to the following differential equation with initial and reflecting boundary conditions:

$$\frac{d}{dt} S_{\text{ex}}(t|\gamma_0) = L_{\gamma_0}^+ S_{\text{ex}}(t|\gamma_0) - k_f(\gamma_0) S_{\text{ex}}(t|\gamma_0),$$

$$S_{\text{ex}}(0|\gamma_0) = \frac{1}{2\pi R^2(1 + \cos(\gamma_0))}, \quad (4)$$

$$\left. \frac{d}{dt} S_{\text{ex}}(t|\gamma_0) \right|_{\gamma_0=\gamma_m} = 0,$$

where t is time and γ_0 is the initial angular position of the acceptor with respect to the donor. γ_m is the minimum angle, which occurs when the donor and acceptor are in contact. $L_{\gamma_0}^+$ is the adjoint of the Smoluchowski diffusion operator,

$$L_{\gamma_0}^+ = \frac{1}{R \sin \gamma_0} \exp\left(\frac{V(\gamma_0)}{k_B T}\right) \frac{d}{d\gamma_0} D(\gamma_0) \frac{\sin \gamma_0}{R} \times \exp\left(-\frac{V(\gamma_0)}{k_B T}\right) \frac{d}{d\gamma_0}, \quad (5)$$

where $D(\gamma_0)$ is the distance dependent diffusion coefficient. It accounts for the hydrodynamic effect,^{30,34–36,46} which describes the reduction in the diffusion constant as the donor and acceptor approach. k_B is Boltzmann’s constant, T is temperature, and $V(\gamma_0)$ is the distance dependent potential in which the acceptors are diffusing. Because there is no Coulomb interaction for either the initial species or the radicals, $V(\gamma_0)$ is only the potential of mean force, which is determined by the radial distribution function, $V(\gamma_0) = -\ln[g(\gamma_0)]$.³⁵ $k_f(\gamma_0)$ in Eq. (1) is the rate of the forward electron transfer described by the Marcus-Hush equations:^{47–50}

$$k_f(r) = \frac{2\pi}{\hbar} J_f^2 \exp[-\beta_f(r - r_m)] \frac{1}{\sqrt{4\pi\lambda_f k_B T}} \times \exp\left[\frac{-(\Delta G_f + \lambda)^2}{4\lambda_f k_B T}\right], \quad (6)$$

where \hbar is Planck’s constant divided by 2π and r_m is the contact distance. r is given in terms of the angular parameter γ in Eq. (1). The donor-acceptor electronic coupling for forward transfer is characterized by J_f , the magnitude of coupling at contact, and β_f , which reflects the exponential distance dependence of the coupling. $\lambda_f(r)$ is the reorganization energy, which is the combined inner sphere and outer sphere portions. The outer sphere reorganization energy has been calculated for a micelle system, in which all space is divided into regions with distinct dielectric properties.³⁷ ΔG is the free energy change of transfer, which has also been calculated to account for the heterogeneous medium of micelle.³⁷

The excited state survival probability for one donor and n acceptors is obtained as an ensemble average of survival probabilities for one donor and one acceptor:

$$\langle P_{\text{ex}}(t) \rangle_n = e^{-t/\tau} \left[\int_{\gamma_m}^{\pi} S_{\text{ex}}(t|\gamma_0) 2\pi R^2 \sin(\gamma_0) g(\gamma_0) d\gamma_0 \right]^n. \quad (7)$$

Here, τ is the fluorescence lifetime of the donor in the absence of electron transfer. $g(\gamma_0)$ is the solvent radial distri-

bution function used to describe the distribution of acceptors around donor molecules. The number of acceptors in a micelle is assumed to follow a Poisson distribution around N , the mean number of micelle bound acceptors per micelle. Then, the observable $\langle P_{\text{ex}}(t) \rangle$ is

$$\langle P_{\text{ex}}(t) \rangle = \sum_{n=0}^{\infty} \frac{e^{-N} N^n}{n!} \langle P_{\text{ex}}(t) \rangle_n. \quad (8)$$

The survival probability for radicals produced from forward electron transfer is more complicated to calculate because the kinetics of the backward transfer are coupled to those of the forward. The final result is

$$\langle P_{\text{ex}}(t) \rangle = N \int_{\gamma_m}^{\pi} \int_0^t S_{\text{ct}}(t-t' | \gamma_0) k_f(\gamma_0) S_{\text{ex}}(t' | \gamma_0) \times P_{\text{ex}}(t') dt' 2\pi R^2 g(\gamma_0) \sin \gamma_0 d\gamma_0. \quad (9)$$

S_{ct} is obtained using an equation identical to Eq. (4). However, instead of the reaction rate coefficient for forward transfer k_f , the backward transfer rate coefficient k_b is used. Because the backward reaction is in the inverted Marcus regime, Eq. (6) is not appropriate. A convenient treatment, developed by Jortner,⁵¹ accounts for high frequency modes of the donor and acceptor molecules. Jortner assumes that these multiple modes can be approximated by a single average high frequency mode. The rate of the backward reaction then becomes:^{39,52,53}

$$k_b = \frac{2\pi}{\hbar \sqrt{4\pi\lambda_S(R)} k_B T} J_b^2 \exp(-\beta_b(R-R_m)) \times \sum_{n=0}^{\infty} \frac{e^{-S} S^n}{n!} \exp\left(\frac{-(\Delta G_b(R) + \lambda_S(R) + nh\nu)^2}{4\lambda_S(R) k_B T}\right), \quad (10)$$

with $S = \lambda_V/h\nu$. J_b is the magnitude of coupling at contact for the backward transfer, and β_b determines the distance dependence for the back transfer. λ_V is the reorganization energy associated with the mean high frequency mode, while λ_S is the classical solvent reorganization energy. $\Delta G_b(R)$ is the free energy change for the backward transfer process.

B. Input parameters

The donor and acceptor radii were obtained as the radii of spheres having the same volumes as the donor and acceptor. For ODRB the hydrocarbon tail was excluded. The radius for ODRB is 4.12 Å and for DMA, 2.75 Å. The contact distance r_m between ODRB and DMA is 6.87 Å.

The micelle radius represents the distance from the center of the micelle to the center of the donor and acceptor molecule (see Fig. 4). It is taken to be the core radius determined by the Tanford equation: $R = 1.5 + 1.265n_C$ Å, where n_C is the number of carbons in the hydrocarbon tail.⁵⁴ The model assumes that all donors and acceptors are located in the micelle head group region. Both simulations and experiments give micelle head group region thicknesses of 5–9 Å.^{55–57} The donor and acceptors are modeled to be in the center of the head group region. Therefore, for convenience, we take the thickness of the head group region to be

the diameter of ODRB. Then, the radius of the core is $a_c = R - 4.12$ Å, and the radius of the head group water interface is $a_s = R + 4.12$ Å. The optical and static dielectric constants of the micelle's hydrocarbon core were taken to be the constants for hexane, $\epsilon_{\text{op}} = \epsilon_{\text{st}} = 1.88$.⁵⁸ The constants of water surrounding the micelles are $\epsilon_{\text{op}} = 1.77$ and $\epsilon_{\text{st}} = 78.3$.⁵⁸ The optical dielectric constant for the head group region was taken to be $\epsilon_{\text{op}} = 1.9$. The static dielectric constant of the head group region has been varied in the fitting process. The dielectric constants are used to calculate both solvent reorganization energy and free energy of transfer in micelles employing the procedures developed specifically for micelles.³⁷

The difference between the reduction potential of rhodamine B and the oxidation potential of DMA in acetonitrile, as measured by cyclic voltammetry, is 1.55 V.³⁸ The frequency of the excitation has been determined as the frequency of the pump beam, $\nu = 565$ nm. These values were used to calculate ΔG following the method developed for the three region dielectric environment of the micelle head groups.³⁷

The diffusion constant of DMA in the micelle head group region was determined to be $D = 15$ Å²/ns.³⁶ Since ODRB molecules are tethered into the micelles, their diffusion is insignificant compared to that of DMA. The value of D was varied to some extent in the fitting of the data.

V. COMPARISON BETWEEN DATA AND THEORY

A. Forward transfer dynamics

The theoretical model was used to fit the $P_{\text{ex}}(t)$ experimental data by varying four unknown parameters: J_f , β_f , ϵ_{st} , and σ , the effective diameter of the solvent in the micelle head group region that determines the radial distribution function of the acceptors about the donor. (A detailed discussion of the radial distribution function as used in the determination of the donor-acceptor electron transfer in solution has been given^{28,29}). It has been demonstrated that the solute radial distribution function tracks that of the solvent for relatively low solute concentrations in regular liquids.⁵⁹ It is assumed that the regular liquid results also apply to the head group region of the micelles. Therefore, the radial distribution function of the solvent (head group molecular makeup) was used but adjusted for the donor-acceptor contact distance, which is the sum of the R3B and DMA radii. The value of ϵ_{st} has been varied between the value of dielectric constant in micelle's core ($\epsilon_{\text{st}} = 1.88$) and the value in water ($\epsilon_{\text{st}} = 78$). σ was varied in the 1–7 Å range. The parameter β_f has been previously found to be ~ 1 Å⁻¹ in a wide variety of systems.^{53,60–62} We used this value of β_f , but varied the coupling constant J_f in the 10–1000 cm⁻¹ range.

In a previous study, $P_{\text{ex}}(t)$ was obtained from the decays of ODRB fluorescence in the presence of varying concentrations of DMA.³⁶ The experimental results were fit to the model using $J_f = 300$ cm⁻¹, $\sigma = 5$ Å, and $\epsilon_{\text{st}} = 30$. In the current study, we initially used the same parameters to fit the forward data. The previous and current experimental setups differ in their time resolution, which was improved from 50 ps in the previous setup to 0.2 ps in the current setup. Figures 5(a) and 5(b) show the data and calculated curves for

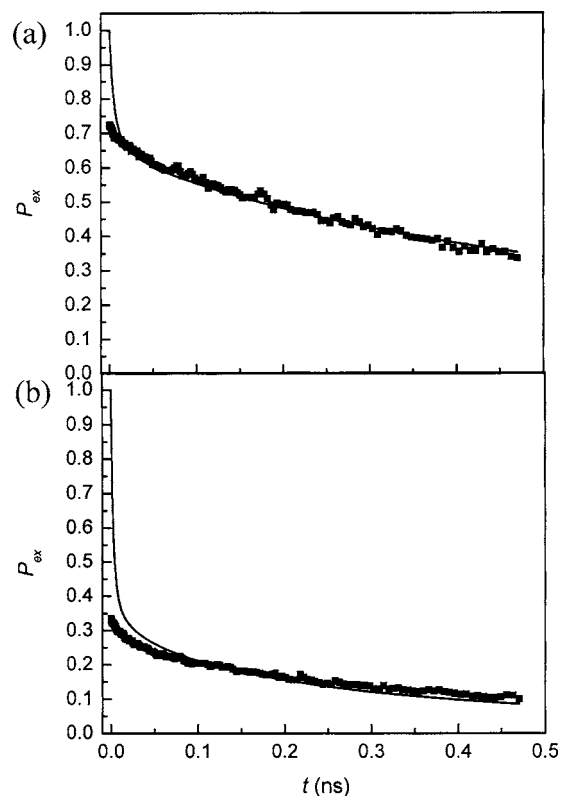


FIG. 5. (a) and (b) show the data for 3 and 6 mM DTAB samples, respectively. The solid curves are calculated from parameters found in previous experiments that did not have sufficient time resolution to access time < 100 ps.

3 mM and 6 mM DTAB samples, respectively. The fits are in good agreement with the current data at times longer than ~ 50 ps, suggesting that the two experimental setups reproduce well the decay curves. However, the parameters obtained from the previous experiments overestimate the rate of the forward transfer at short times. This discrepancy is due to a lack of the sufficient time resolution in the previous experiments, making the fits insensitive to the short time dynamics.

Figure 6 displays data and fits for the DTAB micelle with the two lowest DMA concentrations [3 mM (a) and 6 mM (b)]. The fits to the TTAB data are similar in appearance. The values for the parameters obtained from the fits are given in Table I. The quality of the fits is reasonably good. For each micelle, the values of the parameters for the two lowest concentrations are the same, although the parameters are different for the highest concentrations (see below). The values of some of the fitting parameters are significantly different for DTAB and TTAB. The coupling constant J_f is larger in DTAB micelles than in TTAB micelles. Also, the dielectric constant of the micelle head group region is higher in DTAB micelles. The dielectric constant in the head group is $\epsilon_{st}=30$ for DTAB micelles and 10 for TTAB micelles, which indicates that the dielectric constant decreases as the size of the micelle increases. The difference in the dielectric constants can arise because of differences in the micelles' structures. The smaller micelle, DTAB, has a more "open" structure that can permit more water penetration into the head group region.⁶³ An increase in water concentration in

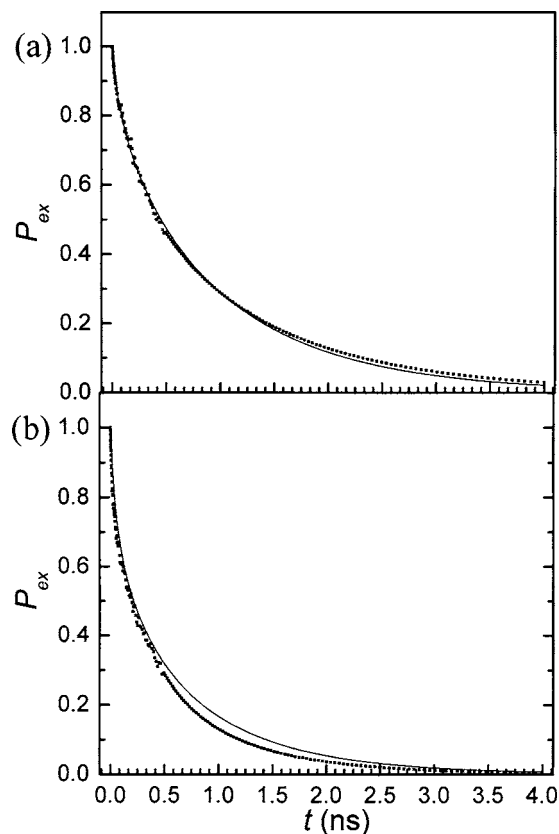


FIG. 6. Data and fits for the DTAB micelle with the two lowest DMA concentrations [(a) 3 mM and (b) 6 mM]. The fits to the TTAB data are similar in appearance. The values for the parameters obtained from the fits are given in Table I. The quality of the fits is reasonably good.

the head group region will increase the dielectric constant. This is consistent with the results obtained from neutron scattering studies that have shown that there are more methylene units in contact with water in the smaller trimethylammonium bromide micelles and the water penetrates deeper in the smaller micelles.⁶³

The solvent diameter in the micelle's head group is found to be $\sigma=2$ Å. This value is lower than the diameter of the surfactant head groups, and is close in value to the diameter of water molecules. This result suggests that the donor and acceptor molecules involved in the electron transfer process are separated only by water molecules and not by the surfactant head groups. Since the estimated center-to-center distance between ODRB and the first neighboring surfactant molecule is ~ 10 Å, all the DMA molecules involved in elec-

TABLE I. Parameters used to fit the forward electron transfer data.

Sample ^a (mM)	J_f (cm ⁻¹)	σ (Å)	ϵ_{st}	DMA (%) ^b
DTAB, 3	20	2	30	40
DTAB, 6	20	2	30	40
DTAB, 12	40	2	38	35
TTAB, 3	15	2	10	40
TTAB, 6	15	2	10	40
TTAB, 12	30	2	38	35

^aMicelle type followed by concentration of DMA.

^bPercentage of DMA bound to micelle.

tron transfer are within this radius around ODRB. This is consistent with the fact that the DMA diffuses slowly in micelles, while ODRB does not diffuse at all.

Even though the portion of DMA molecules that incorporates the micelle's head group region has been experimentally obtained, the uncertainty of the measurement is high. For this reason, we allowed this value to vary during the fitting process. We found that the values obtained from the fit are somewhat lower than the value of 57% bound DMA obtained in a previous measurement.³⁶ The value obtained from the fits is 40% DMA bound for both DTAB and TTAB micelles. It is not clear if this difference is outside the range of experimental error.

There is no obvious reason for the J_f values to differ because J_f might be expected to be a property of the specific donor-acceptor system and more or less independent of the medium. Attempts to fit the experimental results using the same J_f for two micelle systems by varying other parameters, such as distance dependent constant β_f , micelle radius R , effective solvent diameter σ , diffusion constant D , and percent of DMA molecules bound to micelles, were unsuccessful.

The values obtained for the coupling constants J_f (20 cm⁻¹ for DTAB and 15 cm⁻¹ for TTAB), are lower than the value obtained in a recent study of electron transfer between rhodamine 3B (ethyl ester rather than octadecyl ester) and DMA in three liquid solvents, where it was found that $J_f=180, 90,$ and 55 cm⁻¹ in acetonitrile, butyronitrile, and benzonitrile, respectively.²³ A possible explanation for the difference in J_f between the liquids and the micelles might be a restricted orientational configuration imposed on the donor and acceptor by the nature of ODRB and the surfactant environment of the micelle head group region. In the theoretical model, there is no angular dependence in the electronic interaction matrix element. In a liquid solution, the forward transfer process begins with the donors and acceptors having a random distribution of orientations and a very broad range of separations determined by the concentration and the radial distribution function. Some of the orientations are undoubtedly more favorable than others; that is, the electronic interaction is a function of angles. However, all angles are present, and while orientational relaxation will take unfavorable orientations into favorable orientations, it will also take favorable orientations into unfavorable ones. In a theoretical study of forward electron transfer, the combined influence of a distribution of distances and orientations without orientational and spatial diffusions was studied.⁶⁴ It was found that the time dependence of electron transfer with both angular and distance dependent transfer rates was not significantly different in functional form from the time dependence with a distance dependence only if the distance dependent parameters were changed only slightly.⁶⁴ In the absence of an exact knowledge of the distance dependences, the orientational dependence is washed out in liquids. Therefore, J_f determined in liquids is an orientationally averaged value.

However, the ODRB chromophore head group essentially spans the micelle head group region. It is expected that the charged amine substituents (single charged with two resonance structures) on the aromatic rings will be close to or

will project into the water at the surface of the micelle. Because of the long hydrocarbon tail of ODRB, which will be part of the micelle core, combined with the tendency of the charges to seek the water boundary, the ODRB orientational distribution is likely not to be random. DMA is not charged and does not have a hydrocarbon tail anchor. It will assume all orientations in the head group region. Therefore, a ODRB/DMA pair may not sample all relative orientations with equal probability, and if the most probable accessible orientations are unfavorable, the ensemble averaged J_f will be reduced compared to a liquid solution of R3B and DMA. TTAB, which has a more tightly packed structure and fewer water molecules in the head group region, may further restrict the angular relationship to even more unfavorable configurations, resulting in the observed smaller J_f value. The explanation for different values of J_f is reasonable, but it is only a conjecture.

Another possible explanation for the smaller values of J_f obtained in the micelle solutions with respect to the results obtained in liquids might be that the range of donor-acceptor distances are skewed in micelles. As mentioned above, the ODRB chromophore is approximately as large as the head group region, and the charges will pin it to the water interface. DMA is considerably smaller and uncharged and only somewhat polar. It might tend to reside on average deeper in the head group region, perhaps at the interface with the core. The theoretical model assumes that the donor and acceptors are located with their centers on a spherical shell that is centered in the head group shell. The difference between the geometry of the model and possible deviations from it in terms of the true spatial distribution of the donors and acceptors in the head group region would change the distribution of distances in the spatial average. Since the electron transfer rate falls off exponentially with distance, the electronic coupling constant obtained from the fits could be smaller.

The fits are not close to perfect. Various parameters are not known accurately and must be fitted. Although the theoretical model includes many important aspects that differentiate a liquid from a micelle in the context of electron transfer, the differences in observed J_f s between the liquid samples and the two micelle samples may arise from an incomplete description of the nature of the micelle environment as reflected in the discussions of possible orientational restrictions and possible spatial distributions not described as donor and acceptor distributed on a single spherical shell.

The same parameters fitted the lower two concentrations for each micelle, although the parameters differed somewhat between the micelles. However, the samples with highest DMA concentration (12 mM DMA) gave a different set of fitting parameters. The data and fit are shown in Fig. 7 for DTAB. In addition to the data and the fit through the data, the other solid curve is the calculation for 12 mM DMA using the same parameters that fit the lower two concentrations. The results for TTAB behave similarly. The three DMA concentrations studied correspond to an average number of DMA incorporated into the micelles of approximately 9, 18, and 36 based on the previous study of the percent of binding³⁶ and the fitting for the lower two DMA concentrations. For the highest concentration, the heavy loading of the

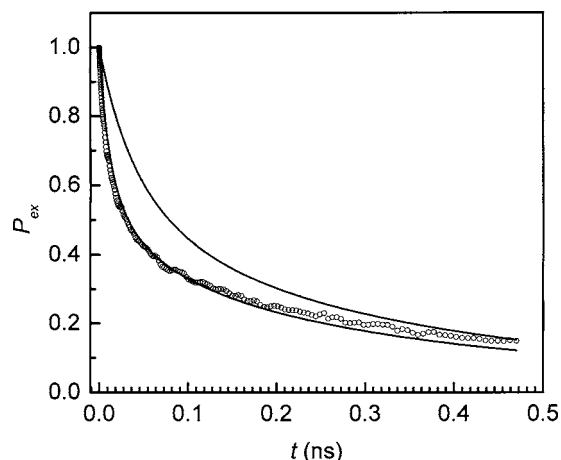


FIG. 7. The data (circles) and fit are shown for 12 mM DMA for DTAB. In addition to the data and the fit through the data, the other solid curve is the calculation for 12 mM DMA using the same parameters that fit the lower two concentrations shown in Fig. 6.

micelles with DMA can lead to the deformation of the micelles. The NMR studies of aromatic molecules in micelle systems show that, at low concentrations, aromatics tend to localize in the micelle's head group region.⁶⁵⁻⁶⁷ However, at higher concentrations, the micelle's spherical geometry is disturbed. Studies on benzene molecules suggest that benzene penetrates deeper into the micelle, producing a pool in the center (microemulsion).⁶⁵ Other studies on alkylbenzenes suggest that aromatic molecules decrease the surface charge density of micelles, reducing the repulsive interactions between micelles which in turn leads to growth from spherical to rodlike micelles.^{66,67}

It is unclear to what extent if any the high concentration of DMA influences the micelles' structure. If the micelles are deformed, the deformation has a significant impact on the electron transfer. Forward electron transfer is faster as is clear from the data in Fig. 7 and the coupling constants obtained from the fits, $J_f=40\text{ cm}^{-1}$ in DTAB micelles and $J_f=30\text{ cm}^{-1}$ in TTAB micelles, which are substantially larger than those obtained from the experiments on the lower concentration DMA samples (see Table I).

B. Geminate recombination dynamics

In analyzing the radical geminate recombination data, only the parameters involved in the calculation of P_{ct} were varied. $P_{ex}(t)$, which goes into the P_{ct} calculation, was determined using the parameters obtained from the stimulated emission decays described in the previous section. There are three unknown fitting parameters: the coupling constant for back electron transfer, J_b , the reorganization energy associated with the mean high frequency mode, λ_V , and the frequency of the mode, ν . To reduce the number of fitting parameters, values for the mean frequency of $\nu=1550\text{ cm}^{-1}$ and the reorganization energy of $\lambda_V=0.4\text{ eV}$ were used. These values are reasonable estimates for aromatic D/A systems. Therefore, only the value for electronic coupling constant J_b was varied.

The fits of the data obtained with samples containing DTAB micelles and the lower two DMA concentrations are

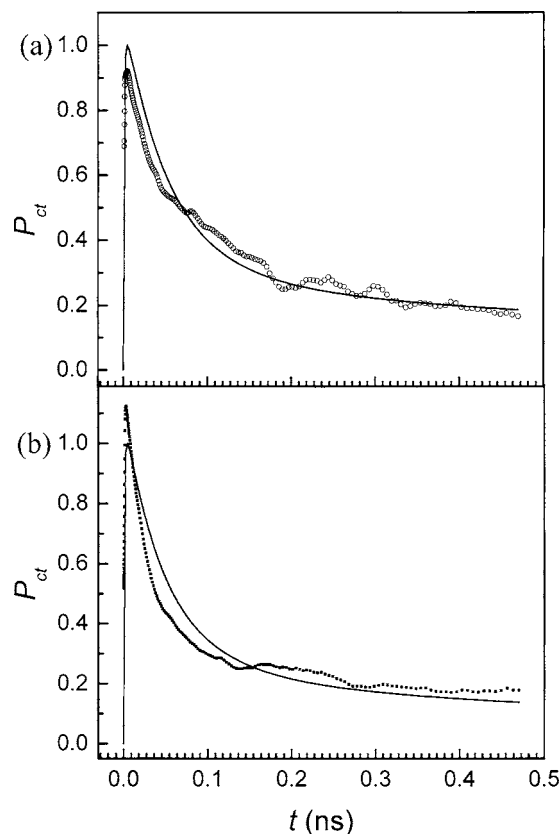


FIG. 8. The radical geminate recombination data, P_{ct} for 3 mM DMA [(a) circles] and 6 mM DMA [(b) squares] in DTAB micelles. The solid curves are calculations using a single adjustable parameter. The functional forms of the calculated curves, while not perfect, are certainly quite reasonable, given that there is only a single adjustable parameter. The results are similar in samples with TTAB micelles.

presented in Fig. 8. The functional forms of the calculated curves, while not perfect, are certainly quite reasonable, given that there is only a single adjustable parameter. The results are similar in samples with TTAB micelles. The coupling constants for the geminate recombination found from the fits are significantly higher ($J_b=200\text{ cm}^{-1}$ for DTAB and 150 cm^{-1} for TTAB micelles) than the values obtained for forward transfer. The geminate recombination rates are higher than the forward electron transfer rates.

It is interesting to compare how the absolute magnitude of the radical signal changes with the increasing DMA concentrations. The experimentally obtained radical curves do not allow us to compare the amplitudes of radical signals obtained in different measurements because of variations in the experimental conditions, such as: (i) the concentration of ODRB in each sample, (ii) the power of the pump beam in each measurement, and (iii) the pump-probe overlaps in each sample. However, the theoretical simulation of P_{ct} curves using the parameters obtained from the fits to the experimental data makes the comparison of different P_{ct} values possible. Figure 9 presents the unscaled P_{ct} curves for three different DMA concentrations obtained using the same parameters as in Fig. 8. As expected, the increased concentration of DMA gives rise to larger build up of radical molecules in solution. The reason for this behavior lies in the fact that the k_f value falls off faster with distance than does

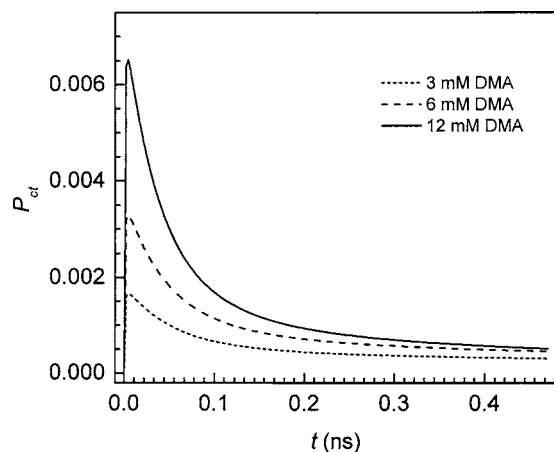


FIG. 9. The radical geminate recombination calculations, P_{ct} , for 3 mM DMA (short dashes), 6 mM DMA (long dashes), and 12 mM DMA (solid) in DTAB micelles. The parameters used are the same as the ones obtained by fitting the experimental curves. P_{ct} curves with higher DMA concentrations exhibit a greater buildup of radicals. The same trend is obtained for calculations in TTAB micelles.

k_b . At high DMA concentrations, the average D-A distance is small and the rates of k_f and k_b are large. The exact values of these rate constants determine the quantity of the radical molecules that build up. At lower DMA concentrations, the average D-A distance is large, which leads to a decrease in both k_f and k_b values. However, the k_f value exhibits a faster decrease with distance than does k_b , leading to a smaller quantity of radicals accumulated in solution.

It is interesting to consider possible reasons why the J_f 's are so much smaller than the J_b 's. Two possibilities were discussed above in connection with the small values found for J_f 's in micelles. The first was that the relative D-A orientational configurations in micelles are restricted and limit the probability of the donor and acceptors obtaining configurations that produce the largest electronic interactions. Because the observed J_f is an ensemble average over orientations, it is possible that limiting the distribution of relative donor-acceptor orientations could produce a reduced J_f . To explain the larger micelle J_b 's, it would be necessary to propose that the allowed configurations, which are unfavorable for forward transfer, produce a distribution of radical pair orientational configurations that are just the opposite; that is, the distribution that produces small J_f 's gives large J_b 's. This is possible because different electronic states are involved in the forward and backward transfer processes. This is a conjecture that might be tested with electronic structure calculations that would be very difficult because such calculations involve excited states and radical states interacting on different molecules.

The other possibility discussed in connection with the forward transfer interactions involved the donor and acceptors not being distributed on a spherical shell in the center of the head group region, the configuration used in the calculations. If the acceptors tend to be deeper in the head group region, the spatial average is incorrect. The physical system on average has the acceptors further from the donor than in the model, producing slower forward transfer. To fit the data, the calculation would produce J_f 's that are smaller than the

true contact value. The effect of the skewed spatial distribution on the geminate recombination rates might be less pronounced. Because the geminate recombination occurs in the inverted Marcus region, the distance dependence is not the same as in the normal region of the forward transfer. In the inverted region, there are two competing effects that interplay in determining the distance dependence of the transfer. One effect is the exponential decay of rate with distance as in forward electron transfer. The other effect leads to an increase in the reaction rate with distance and is related to an increase in the reorganization energy with distance, pushing the reaction into the normal Marcus region. The overall effect of these two processes leads to a shallower distance dependence for geminate recombination than for the forward electron transfer. Then, a possible skewed distribution of distances may have less effect on the model's ability to fit the data with reasonable parameters for backward transfer than for forward transfer.

VI. CONCLUDING REMARKS

In this paper we presented the first measurements of geminate recombination of radical following photoinduced forward electron transfer between a donor and acceptors located in the head group regions of two micelle systems. In addition, the study of the forward transfer was extended to shorter times than previous measurements on micelles. The nature of the forward transfer and of the geminate recombination were illustrated with concentration dependent data and discussed qualitatively.

The data were analyzed using a detailed theory of forward electron transfer and geminate recombination in the head group region of micelles. The theoretical treatment includes many important aspects that make electron transfer in micelles different from electron transfer between donors and acceptors in normal liquid solvents.^{36,37} The model accounts for the nonisotropic nature of the dielectric medium, which influences the free energy and the reorganization energy.³⁷ The model also includes the influence of diffusion and solvent structure in the head group region. The theoretical calculations were able to reproduce the shapes of the forward and backward transfer data with reasonable fidelity and parameters. The forward transfer electronic coupling matrix elements were much smaller than the corresponding backward transfer matrix elements. Two possibilities were discussed that might account for this seeming anomaly. These conjectures really point to the additional complexity of modeling electron transfer in complex media in which all of the structural aspects of the system are not known.

ACKNOWLEDGMENTS

One of the authors (A.G.) thanks the W. M. Keck Foundation for support. This research was funded by the Department of Energy DE-FG03-84ER13251.

¹R. B. Gregory, *Protein Solvent Interactions* (Marcel Dekker, New York, 1995).

²L. D. Barron, L. Hecht, and G. Wilson, *Biochem.* **36**, 13143 (1997).

³W. S. G. A. Jeffrey, *Hydrogen Bonding in Biological Structures* (Springer-Verlag, Berlin, 1991).

- ⁴R. R. S.-H. Chen, *Micellar Solutions and Microemulsions: Structure, Dynamics and Statistical Thermodynamics* (Springer-Verlag, New York, 1990).
- ⁵M. P. Pileni, *Structure and Reactivity in Reverse Micelles* (Elsevier, Amsterdam, 1989).
- ⁶P. B. Stig and E. Friberg, *Microemulsions: Structure and Dynamics* (CRC, Boca Raton, FL, 1987).
- ⁷R. M. Dickson, A. B. Cubitt, R. Y. Tsien, and W. E. Moerner, *Nature* (London) **388**, 355 (1997).
- ⁸R. M. Dickson, D. J. Norris, Y.-L. Tzeng, and W. E. Moerner, *Science* **274**, 966 (1996).
- ⁹R. Breslow and S. D. Dong, *Chem. Rev. (Washington, D.C.)* **98**, 1997 (1998).
- ¹⁰M. A. Fox, *Top. Curr. Chem.* **159**, 67 (1991).
- ¹¹D. G. Whitten, J. C. Russell, and R. H. Schmehl, *Tetrahedron* **38**, 2455 (1982).
- ¹²G. Jerke, J. S. Pedersen, S. U. Egelhaaf, and P. Schurtenberger, *Phys. Rev. E* **56**, 5772 (1997).
- ¹³O. A. ElSeoud, *J. Mol. Liq.* **72**, 85 (1997).
- ¹⁴I. R. Piletic, H. S. Tan, and M. D. Fayer, *J. Phys. Chem. B* **109**, 21273 (2005).
- ¹⁵H. S. Tan, I. R. Piletic, and M. D. Fayer, *J. Chem. Phys.* **122**, 174501 (2005).
- ¹⁶N. M. Correa, E. N. Durantini, and J. J. Silber, *J. Phys. Org. Chem.* **18**, 121 (2005).
- ¹⁷X. G. Meng, Y. Guo, C. W. Hu, and X. C. Zeng, *J. Inorg. Biochem.* **98**, 2107 (2004).
- ¹⁸M. Al-Sheikhly, J. Silverman, M. Simic, and B. Michael, *J. Phys. Chem. B* **108**, 17618 (2004).
- ¹⁹A. Muller, *Electron and Proton Transfer in Chemistry and Biology* (Elsevier, Amsterdam, 1992).
- ²⁰H. Hoppe and N. S. Sariciftci, *J. Mater. Res.* **19**, 1924 (2004).
- ²¹M. Tachiya and A. Mozumder, *Chem. Phys. Lett.* **28**, 87 (1974).
- ²²M. Tachiya, *Radiat. Phys. Chem.* **21**, 167 (1983).
- ²³A. Goun, K. Glusac, and M. D. Fayer, *J. Chem. Phys.* **124**, 084504 (2006).
- ²⁴Y. Lin, R. C. Dorfman, and M. D. Fayer, *J. Chem. Phys.* **90**, 159 (1989).
- ²⁵R. C. Dorfman, Y. Lin, and M. D. Fayer, *J. Phys. Chem.* **94**, 8007 (1990).
- ²⁶R. C. Dorfman and M. D. Fayer, *J. Chem. Phys.* **96**, 7410 (1992).
- ²⁷S. F. Swallen and M. D. Fayer, *J. Chem. Phys.* **103**, 8864 (1995).
- ²⁸S. F. Swallen, K. Weidemaier, and M. D. Fayer, *J. Chem. Phys.* **104**, 2976 (1996).
- ²⁹S. F. Swallen, K. Weidemaier, H. L. Tavernier, and M. D. Fayer, *J. Phys. Chem.* **100**, 8106 (1996).
- ³⁰K. Weidemaier, H. L. Tavernier, S. F. Swallen, and M. D. Fayer, *J. Phys. Chem. A* **101**, 1887 (1997).
- ³¹H. L. Tavernier, M. M. Kalashnikov, and M. D. Fayer, *J. Chem. Phys.* **113**, 10191 (2000).
- ³²V. O. Saik, A. A. Goun, J. Nanda, K. Shirota, H. L. Tavernier, and M. D. Fayer, *J. Phys. Chem. A* **108**, 6696 (2004).
- ³³V. O. Saik, A. A. Goun, and M. D. Fayer, *J. Chem. Phys.* **120**, 9601 (2004).
- ³⁴J. M. Deutch and B. U. Felderhof, *J. Chem. Phys.* **59**, 1669 (1973).
- ³⁵S. H. Northrup and J. T. Hynes, *J. Chem. Phys.* **71**, 871 (1979).
- ³⁶H. L. Tavernier, F. Laine, and M. D. Fayer, *J. Phys. Chem. A* **105**, 8944 (2001).
- ³⁷H. L. Tavernier, A. V. Barzykin, M. Tachiya, and M. D. Fayer, *J. Phys. Chem. B* **102**, 6078 (1998).
- ³⁸K. Weidemaier, H. L. Tavernier, and M. D. Fayer, *J. Phys. Chem. B* **101**, 9352 (1997).
- ³⁹K. Weidemaier, H. L. Tavernier, K. T. Chu, and M. D. Fayer, *Chem. Phys. Lett.* **276**, 309 (1997).
- ⁴⁰K. Weidemaier and M. D. Fayer, *J. Phys. Chem.* **100**, 3767 (1996).
- ⁴¹K. Weidemaier and M. D. Fayer, *J. Chem. Phys.* **102**, 3820 (1995).
- ⁴²F. Reissshusson and V. Luzzati, *J. Phys. Chem.* **68**, 3504 (1964).
- ⁴³P. C. Beaumont, D. G. Johnson, and P. J. Parsons, *J. Photochem. Photobiol., A* **107**, 175 (1997).
- ⁴⁴M. D. Ediger, R. P. Domingue, and M. D. Fayer, *J. Chem. Phys.* **80**, 1246 (1984).
- ⁴⁵J. C. Eriksson and G. Gillberg, *Acta Chem. Scand. (1947-1973)* **20**, 2019 (1966).
- ⁴⁶R. Zwanzig, *Adv. Chem. Phys.* **15**, 325 (1969).
- ⁴⁷R. A. Marcus, *Annu. Rev. Phys. Chem.* **15**, 155 (1964).
- ⁴⁸N. S. Hush, *Trans. Faraday Soc.* **57**, 557 (1961).
- ⁴⁹R. A. Marcus, *J. Chem. Phys.* **24**, 966 (1956).
- ⁵⁰R. A. Marcus, *J. Chem. Phys.* **24**, 979 (1956).
- ⁵¹J. Jortner, *J. Chem. Phys.* **64**, 4860 (1976).
- ⁵²R. A. Marcus and N. Sutin, *Biochim. Biophys. Acta* **811**, 265 (1985).
- ⁵³J. R. Miller, J. V. Beitz, and R. K. Huddleston, *J. Am. Chem. Soc.* **106**, 5057 (1984).
- ⁵⁴C. Tanford, *J. Phys. Chem.* **76**, 3020 (1972).
- ⁵⁵L. Laaksonen and J. B. Rosenholm, *Chem. Phys. Lett.* **216**, 429 (1993).
- ⁵⁶K. Watanabe, M. Ferrario, and M. L. Klein, *J. Phys. Chem.* **92**, 819 (1988).
- ⁵⁷S. S. Berr, *J. Phys. Chem.* **91**, 4760 (1987).
- ⁵⁸J. A. R. W. B. Bunger, *Organic Solvents: Physical Properties and Methods of Purification* (Wiley, New York, 1986).
- ⁵⁹G. J. Throop and R. J. Bearman, *J. Chem. Phys.* **44**, 1423 (1966).
- ⁶⁰G. L. Closs and J. R. Miller, *Science* **240**, 440 (1988).
- ⁶¹G. Angulo, G. Grampp, A. A. Neufeld, and A. I. Burshtein, *J. Phys. Chem. A* **108**, 6667 (2003).
- ⁶²V. S. Gladkikh, A. I. Burshtein, H. L. Tavernier, and M. D. Fayer, *J. Phys. Chem. A* **106**, 6982 (2002).
- ⁶³S. Berr, R. R. M. Jones, and J. S. Johnson, *J. Phys. Chem.* **96**, 5611 (1992).
- ⁶⁴R. P. Domingue and M. D. Fayer, *J. Chem. Phys.* **83**, 2242 (1985).
- ⁶⁵N. Hedin, R. Sitnikov, I. Furo, U. Henriksson, and O. Regev, *J. Phys. Chem. B* **103**, 9631 (1999).
- ⁶⁶P. M. Lindemuth and G. L. Bertrand, *J. Phys. Chem.* **97**, 7769 (1993).
- ⁶⁷A. Heindl, J. Strand, and H. H. Kohler, *J. Phys. Chem.* **97**, 742 (1993).